Dynamic Spot Diffusing Configuration for Indoor Optical Wireless Access

Farhad Khozeimeh, *Graduate Student Member, IEEE*, and Steve Hranilovic, *Senior Member, IEEE*

Abstract—This paper introduces the *dynamic spot diffusing* (DSD) configuration for high-speed indoor wireless optical communications. In this configuration, data are modulated onto a moving spot which is translated over the ceiling. A multi-element imaging receiver is pointed upward and acquires data whenever the transmitter spot is in its field-of-view (FOV). We develop expressions for the channel capacity of such DSD links and discuss design techniques to maximize these information theoretic bounds. Rather than tracking the transmitter spot, we apply rateless erasure correcting codes to approach the capacity of the simulated DSD links. This technique is demonstrated to have better flexibility, greater multipath immunity, higher data rates and simpler transmitters than previously defined multi-spot and diffuse architectures. In a $6 \times 6 \times 3$ m room, simulated data rates vary between 7 Mbps to 25 Mbps at different positions using a single 100 Mbps transmitter and between 35 Mbps to 84 Mbps using 6 spots and the designed erasure correction code. Using power efficient modulation and power gain due to the spot motion of the DSD system, proportionally higher rates are estimated when faster 1 Gbps and 10 Gbps transmitters are employed.

Index Terms—Wireless infrared channel, indoor diffuse infrared communication, optical intensity modulation, spot diffusing architecture.

I. INTRODUCTION

OPTICAL bands have many intrinsic advantages for indoor wireless communications. Spectrum at optical wavelengths is unregulated worldwide, theoretically enabling very high-speed communications. Emissions are also contained to a given room, thus improving security. However, indoor optical wireless links suffer from multipath distortion which limits the channel bandwidth as well as limited average optical power due to eye and skin safety issues. As a result, many channel architectures have been proposed to address these problems: diffuse, tracked line-of-sight (LOS) and multispot diffusing (MSD) configurations. In this work, we propose a novel architecture for indoor optical wireless links termed the *dynamic spot diffusing* (DSD) channel. This configuration overcomes the multipath and optical power limitations of indoor optical wireless channels and provides high data rates with a relatively simple transmitter and erasure correction coding.

In diffuse wireless optical links, transmitters emit light over a large solid angle and receivers collect the reflected power from surfaces of the room with a wide field-of-view (FOV) detector [1]. Although this configuration permits mobility and robustness to blocking and shadowing, data rates are limited due to multipath distortion. Standard IEEE 802.11 diffuse optical wireless links support maximum rates of 2 Mbps [2] while IrDA advanced infrared (AIr) links have rates less than 4 Mbps [3].

Tracked LOS links transmit data through a low divergence beam to a receiver with a narrow FOV to improve the received optical signal-to-noise ratio (SNR) as well as to eliminate multipath distortion. Previous work has reported tracked links working at rates of up to 1 Gbps [4]–[7]. However, the cost of this configuration is the need for precise alignment and tracking for mobile users which becomes prohibitively difficult as the number of users increases.

The MSD configuration combines the benefits of both LOS and diffuse links [8]–[13]. The transmitter in MSD systems modulates identical data onto several narrow beams to create a stationary array of spots on the ceiling. A receiver ideally images a single spot and decodes the transmitted data. Computer generated holograms have been employed to form arrays of 10×10 spots for this application [14]. Since the receivers in MSD links have smaller FOV's than diffuse links, they collect less multipath distortion and can have simulated bandwidths in excess of 2 GHz [15]. Experimental MSD systems working at 140 Mpbs with a single receiver [16] and 155 Mbps using an multi-element imaging receiver [6] have been reported. In [13] an experimental MSD system operating at 70 Mbps is reported using discrete receiver elements. A line strip arrangement for the spots has also been studied which still offers significant gains over diffuse links at lower complexity [17], [18]. Recently, the design of transceivers able to operate in both diffuse and MSD configurations has also been considered [19].

The *dynamic* spot diffusing configuration introduced here preserves the advantages of MSD links while reducing the complexity of the transmitter. As shown in Fig. 1, the DSD transmitter consists of a single (or few) spots which are translated over the ceiling in a closed path. A stationary, multi-element imaging receiver is pointed to the ceiling and performs combining across the receive elements [12]. The receiver does not track the transmitter spot on the ceiling, but merely receives data whenever the spot is in its FOV. Thus, the spot motion introduces a degree of *fading* at the receiver. In spite of this fading, the channel capacity of the DSD link can be designed to be significant, and rateless erasure
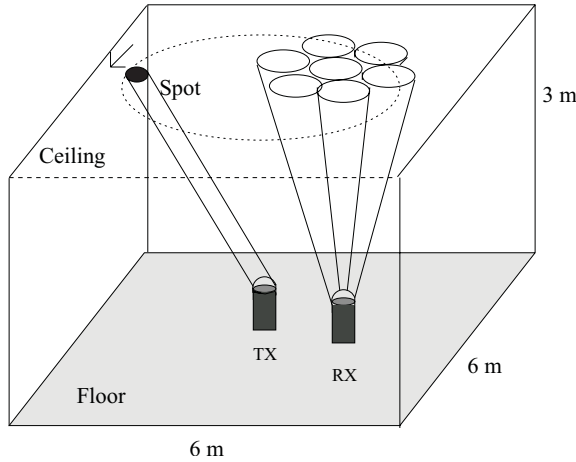
Fig. 1. A dynamic spot diffusing (DSD) link (TX=transmitter, RX=receiver).

correcting codes are applied to achieve high data rates. Due to the robustness of these codes, user mobility is permitted and synchronization to the spot motion is not required. Simulations indicate that with a 100 Mbps modulator and a single transmit beam data rates as high as 25 Mbps are achievable and with a 1 Gbps transmitter and four low complexity transmit beams data rates as high as 840 Mbps are available.

The DSD configuration has several advantages over MSD links. The DSD transmitter is simpler and potentially less expensive than in the MSD case due to the limited number of emitters employed. The spot path of the DSD link can be adapted for any room resulting in a more flexible transmitter than MSD links with fixed computer generated holograms. Fewer spots are required in DSD links to provide coverage over a room than in the case of MSD links. This not only reduces cost, but further reduces the impact of mutipath distortion in DSD links over MSD links, allowing for the use of high speed modulators. Moreover, the movement of the spot relaxes the eye safety power limitation and permits the emission of higher instantaneous optical powers.

This paper is organized as follows. A formal definition of the DSD channel is presented in Sec. II as well as a derivation of the capacity of DSD channels. In Sec. III erasure correcting codes are presented as a practical solution which approach the capacity of the DSD channel. The simulation results for various DSD channels are presented in Sec. IV. Finally, the paper concludes in Sec. V with directions for future work.

II. THE DYNAMIC SPOT DIFFUSING CHANNEL

In DSD links, as shown in Fig. 1, the transmitter consists of one or a few spots which move on the ceiling and are modulated with high bit rate data while the multi-element imaging receiver is oriented toward the ceiling. In this work it is assumed that a spot moves at a constant velocity on a given closed path such as a circle or a line on the ceiling in a periodic manner with period T_s seconds.

A DSD transmitter can be constructed using high-speed laser diodes with a mechanical device to move the beam. Inexpensive translating or rotating mirrors can be used to translate the beam as in commercial laser scanning devices. By controlling the motor speed and mirror orientation the

DSD spot path can be adapted for individual rooms. Micro-electro-mechanical (MEM) systems are another candidate to accomplish beam translation at high speeds. There are many examples of multi-element imaging receivers for indoor wireless optical channels [6], [7], [12]. Rather than having the receiver track the transmitted spot, channel coding techniques are applied to approach the channel capacity in Sec. III. In this section, the DSD channel model is defined and the capacity is derived. System design is then discussed with the aim to maximize the channel capacity of DSD links.

A. DSD Channel Model

Indoor optical wireless links are typically intensity modulated with direct detection (IM/DD) and are modelled by a linear, time-invariant baseband model [12], [20]. Since DSD channels are by definition time-varying, we adopt the generalized linear channel model

$$y(t) = \int_{-\infty}^{\infty} x(\tau)h(t,\tau)d\tau + n(t) \tag{1}$$

where $x(t)$ is the transmitted optical intensity signal, $h(t,\tau)$ is the channel response at time t for an impulse applied at time τ, $y(t)$ is the received photocurrent and $n(t)$ is the channel noise.

The intense ambient illumination of indoor optical wireless links gives rise to high-intensity shot noise, $n(t)$, which can be well modelled as a white, Gaussian, signal-independent noise with variance σ^2 and mean zero [21]. The transmitted signal $x(t)$ is an optical intensity and thus, $x(t) \geq 0$. Additionally, due to eye safety regulations the average amplitude of $x(t)$ must be limited. In this work, we consider binary-level modulation due to its simplicity and the availability of high-speed modulators. A common modulation technique for IM/DD channels is rectangular on-off keying (OOK) [21]. Assuming equally likely bits, the SNR for OOK is defined as [20]

$$\text{SNR}_{\text{OOK}} = \frac{P^2}{R_b \sigma^2}, \tag{2}$$

where P is the average optical power and R_b is the bit rate. The rate $R_b = 1/T_b$, where T_b is the bit period. Power efficient modulation can give a gain in SNR, as discussed in Sec. II-C2.

The time-varying channel impulse response of the DSD channel in (1) can be expanded as

$$h(t,\tau) = h_L(\tau)\delta(t-\tau) + h_M(t,\tau)$$

where $h_L(\tau)$ denotes the LOS component between the spot on the ceiling and the receiver, $h_M(t,\tau)$ is the multipath component and $\delta(\cdot)$ is the Dirac delta functional. In order to compare these two components for DSD channels, the impulse response is simulated in a $6 \times 6 \times 3$ m room with receiver placed at a height of 1 m from the floor, in a configuration identical to previous MSD work [15]. For a fair comparison, in all cases, a single element receiver was used with FOV=11.2° and area 1 cm^2, similar to the one used in [15]. The impulse response of the DSD channel was simulated for a single transmit spot with power equal to a single MSD spot in [15] and is presented for two locations: (i) centered in the receiver FOV and (ii) at maximal distance from the receiver.
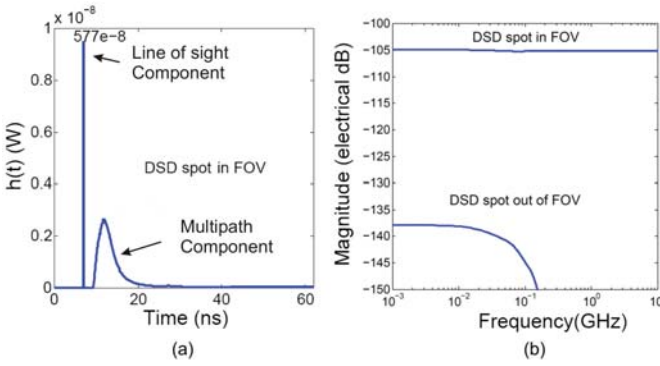
Fig. 2. Impulse response (a) and transfer function (b) for a typical DSD system with spot in and out of receiver FOV.

The impulse responses were simulated using the well known Barry and Kahn algorithm [22] and are presented in Figure 2.

In the DSD architecture, the amount of multipath signals received is negligible in comparison to the LOS component when the spot is in the receiver FOV and the channel is approximately flat to high frequencies. Previous work has shown that the MSD channel has bandwidth in excess of 2 GHz [10], [15]. The DSD system has reduced multipath signal compared to the MSD channel since less spots are employed in the room. In Fig. 2(b) the simulated DSD channel has an approximately flat frequency response up to 10 GHz when spot in FOV of the receiver. When the spot is out of the FOV, the channel DC gain falls by over 30 dB and the bandwidth is reduced over two orders of magnitude. Due to large loss inherent such non-LOS links, we consider transmission in this regime infeasible and model the channel as having a very low channel gain (approaching zero) over the transmission bandwidth. Therefore, the multipath signals can be neglected and the DSD channel can be modelled by solely its channel DC gain at each point in the room up to high frequencies. Thus, we replace $h(t, \tau) = h_L(\tau)\delta(t - \tau)$ in (1) to give the model

$$y(t) = h_L(t)x(t) + n(t). \tag{3}$$

In this work we assume that the receiver has an integrate-and-dump front end, i.e., a matched filter for rectangular OOK. Furthermore, provided that the bit period, T_b, is much smaller than rate at which $h_L(t)$ varies, the channel characteristics can be considered approximately fixed for each bit period. Therefore, the DSD channel can be modelled as a discrete time baseband channel with a fixed channel gain $h_k = h_L(kT_b)$ for each bit period where $k \in \mathbb{Z}$. The channel model (3) can then be simplified to a the discrete time baseband model as

$$y_k = h_k x_k + n_k \tag{4}$$

where y_k is the channel output, x_k is the transmitted optical intensity signal, h_k is the time-varying channel DC gain and n_k channel additive discrete white Gaussian noise.

Due to practical restrictions, the spot motion on the ceiling must follow a fixed closed path such as a circle or a line in a periodic manner with period T_s seconds. Define the set $\mathcal{T}_s = \{1, 2, \ldots, K_s\}$ as the collection of discrete time instants in a single period of spot motion, where $K_s = [T_s/T_b]$ is

the period of spot in discrete time and $[x]$ denotes the integer part of x. Let $\mathcal{T}_{\text{in}} \subseteq \mathcal{T}_s$ denote the set of discrete times when spot is in the FOV in each period and $\mathcal{T}_{\text{out}}$ denote the set of discrete times spot is out of the receiver's FOV in each period. Thus, $\mathcal{T}_{\text{in}} \cap \mathcal{T}_{\text{out}} = \emptyset$ and $\mathcal{T}_{\text{in}} \cup \mathcal{T}_{\text{out}} = \mathcal{T}_s$.

Unlike MSD links, the DSD channel varies in time, even for non-mobile receivers. The channel alternates between two states: a wide bandwidth high SNR channel when the spot is in the FOV of the receiver (i.e.,when $k \in \mathcal{T}_{\text{in}}$) and a low data rate, poor SNR link otherwise (i.e., $k \in \mathcal{T}_{\text{out}}$). The spot motion introduces fading to the DSD channel but also increases the flexibility of the channel and simplifies transmitter design. Note, however, that the data rate in the DSD system is not constant over the room and depends on the position of the receiver, as quantified in Sec. II-B.

B. DSD Channel Capacity

For the DSD channel in (4), the channel gain varies depending on the position of the spot relative to the receiver FOV. For $k \in \mathcal{T}_{\text{in}}$, h_k is high due to the LOS path between the spot on the ceiling and the receiver while for $k \in \mathcal{T}_{\text{out}}$, $h_k \approx 0$. Moreover, for a fixed receiver location, h_k is periodic with period T_s. Therefore, the channel statistics are periodic and the DSD channel is a *cyclo-stationary* channel with period T_s. If the initial phase of spot on its path is a random variable chosen uniformly in $\mathcal{T}_s$, the DSD channel gain can be modelled as a stationary and *ergodic* random process. Therefore, the DSD channel is modelled as a discrete-time channel with stationary and ergodic time-varying gain h_k.

The capacity of ergodic fading channels is a well developed topic [23]. Since the channel state varies, the instantaneous channel capacity also changes in time. For such channels, the *ergodic capacity* is defined as the maximum achievable rate of channel averaged over all channel states [24]. In the DSD channel, channel information is not available at the transmitter since it cannot determine whether the spot is in the FOV of the receiver or not. However, information regarding h_k is potentially available at the receiver since it is possible for receiver to determine whether the spot is in the FOV. This can be done by using a power detector or with a CRC coding technique, discussed in more detail in Sec. III. Therefore, the DSD channel is a flat fading ergodic channel in which channel information is available only at the receiver.

In this work we only consider uniform, binary-level modulations for the DSD channel due to their simple implementation. Specifically, the channel input has a fixed uniform distribution over 0 and $2P$ i.e $x_k \in \{0, 2P\}$. Let $I_b(x_k; y_k)$ denote the mutual information between input and output with this binary, uniform source. Clearly, $I_b(x_k; y_k) \leq 1$ bit/channel use. The ergodic channel capacity of the DSD channel, C_{erg}, for a specific receiver and transmitter configuration is

$$
\begin{aligned}
C_{\text{erg}} &= I_b(x_k; y_k, h_k) \\
&= E_{h_k}[I_b(x_k; y_k|h_k)] \\
&= \frac{1}{K_s}\left(\sum_{k \in \mathcal{T}_{\text{in}}} I_b(x_k; y_k|h_k)) + \sum_{k \in \mathcal{T}_{\text{out}}} I_b(x_k; y_k|h_k))\right)
\end{aligned}
$$

where the last line arises from the fact that h_k is an ergodic and periodic random variable and the expected value can be

replaced by the time average over one period. As discussed in Sec. II-A, since the channel gain is negligible when the spot is out of the FOV

$$C_{\mathrm{erg}} \approx \frac{1}{K_s} \sum_{k \in \mathcal{T}_{\mathrm{in}}} I_b(x_k; y_k | h_k))$$

Define the *channel duration*, C_T, as the fraction of the spot period which spot is the receiver FOV,

$$C_T = \frac{|\mathcal{T}_{\mathrm{in}}|}{K_s},$$

where $|\mathcal{T}_{\mathrm{in}}|$ is the cardinality of $\mathcal{T}_{\mathrm{in}}$. Furthermore, define $C_{\mathrm{in}}^{\mathrm{avg}}$ as the average of instantaneous capacity for $k \in \mathcal{T}_{\mathrm{in}}$. Then, the ergodic capacity can be factored as,

$$C_{\mathrm{erg}} = \underbrace{\frac{|\mathcal{T}_{\mathrm{in}}|}{K_s}}_{C_T} \cdot \underbrace{\frac{1}{|\mathcal{T}_{\mathrm{in}}|} \sum_{k \in \mathcal{T}_{\mathrm{in}}} I_b(x_k; y_k | h_k))}_{C_{\mathrm{in}}^{\mathrm{avg}}} = C_T \cdot C_{\mathrm{in}}^{\mathrm{avg}}.$$

(5)

Following (5), a DSD system must be designed so that it jointly maximizes C_T and $C_{\mathrm{in}}^{\mathrm{avg}}$ for various positions in the room. Notice that in the case of high SNR, $C_{\mathrm{in}}^{\mathrm{avg}} \to 1$ and $C_{\mathrm{erg}}(h_k) \approx C_T$. In this case, the DSD channel to a good approximation behaves as an *erasure* channel. The channel capacity of such an erasure channel with erasure probability $1 - C_T$ is in fact C_T [25]. In the following sections, system design considerations for maximizing $C_{\mathrm{in}}^{\mathrm{avg}}$ and C_T are presented.

C. Maximizing $C_{\mathrm{in}}^{\mathrm{avg}}$

In general, $C_{\mathrm{in}}^{\mathrm{avg}}$ can be increased by improving the average received SNR at the receiver when $k \in \mathcal{T}_{\mathrm{in}}$. This can be accomplished by employing multi-element imaging receivers which reject ambient noise, using more power efficient modulation techniques and by emitting more power at the transmitter.

1) Imaging Receivers: The use of wide FOV single element receivers is limited in indoor optical wireless since they have limited bandwidth and large noise since they collect a great deal of multipath and ambient light. Multi-element receivers are able to reject a portion of received ambient light and improve SNR compared to single element receivers. A convenient implementation is to form *multi-element imaging receivers* comprised of arrays of photodetectors with common imaging optics. A significant gain in average optical power can be realized by combining over the outputs of the receiver array. Two widely used combining techniques are *select best* (SBC) and *maximal-ratio* combining (MRC). In SBC, the receiver which has the highest SNR is selected and its signal is passed as the receiver output. In MRC, signals from all elements are combined using optimal weights to maximize output SNR. A detailed analysis of these combining techniques indicates that gains as high as 15-20 dB optical are possible in non-LOS applications [26].

Multi-element imaging receivers are essential for DSD systems since they permit a large total FOV without incurring large multipath and noise penalties. Although this incurs an increase in complexity, high-speed 100 Mbps multi-element imaging receivers for optical wireless have been reported with higher speed devices under development [7], [27].

2) Power Efficient Modulation Techniques: Power efficient modulation techniques trade bandwidth efficiency for power efficiency by using signals with larger peak-to-average ratios. Pulse position modulation (PPM) is one such example popular in existing optical wireless systems. In L-PPM, a block of L consecutive outputs of an OOK transmitter are assigned such that a non-zero amplitude is transmitted in one slot. Thus, L-PPM can be considered as a rate $\log_2(L)/L$ block code over OOK.

For a given probability of error and bit rate R_b, L-PPM requires $5 \log_{10}(\frac{L \log_2(L)}{2})$ dBo less optical power than OOK [20], [21]. The improvement in optical power efficiency comes at the price of an increase in the required bandwidth over OOK by a factor of $L/\log_2 L$. Hence, for large L, L-PPM can provide significant power gains at the expense of bandwidth efficiency.

Large values of L are not permitted in indoor optical wireless systems due to the multipath induced ISI which limits system performance. As demonstrated in Sec. II, the DSD channel has a very wide bandwidth and as a result, power efficient modulation can be employed to provide a gain in SNR at the receiver without incurring the multipath ISI penalty of non-directed links.

3) DSD Power Gain: All optical wireless systems require tight constraints on the emitted radiation to ensure eye safety. The accessible emission limit (AEL) specifies limits on the average and peak optical power in order to classify systems [28]. The DSD transmitter emits *scanning laser radiation*, i.e., it has a rapidly time-varying direction, as defined in the IEC standard [28, Def. 3.74, pg.18]. Since this is a scanning laser system, at any given point in a room the average optical power that is received is reduced due to the spot motion. In essence the spot motion imposes an effective reduction in the duty cycle of the signal at any fixed point in space. This reduction in duty cycle can be used to increase transmit power, thus improving $C_{\mathrm{in}}^{\mathrm{avg}}$, while remaining eye safe.

Consider the average optical power of the transmitted signal,

$$P = \lim_{T \to \infty} \frac{1}{2T} \int_{-T}^{T} x(t) \, dt.$$

Since the spot has a periodic motion, exposure to the beam is possible for a portion of the spot path period. Let C_T^{eye} denote the portion of each period for which the beam is subtended by an eye. Notice that the received optical power is zero for $1 - C_T^{\mathrm{eye}}$ portion of each period. Thus, the average optical power received by an eye is

$$P_{\mathrm{eye,avg}} = \lim_{M \to \infty} \frac{1}{2M} \int_{-M}^{M} x(t) \cdot C_T^{\mathrm{eye}} \, dt = C_T^{\mathrm{eye}} P. \quad (6)$$

Thus, for the same average optical power the DSD transmitter can have amplitudes $1/C_T^{\mathrm{eye}}$ times that of a fixed-beam MSD system. These larger amplitudes, in turn, increase the capacity $C_{\mathrm{in}}^{\mathrm{avg}}$ when the spot is in the receiver FOV.

Consider the example in Fig. 3. For class 1M operation, eye safety can be verified by measuring the optical power at a distance of 100 mm through a 7 mm aperture which approximates a human pupil [28]. Therefore, C_T^{eye} must be calculated for the worst case that the distance between eye and transmitter is 10 cm. In the example, the transmitter is
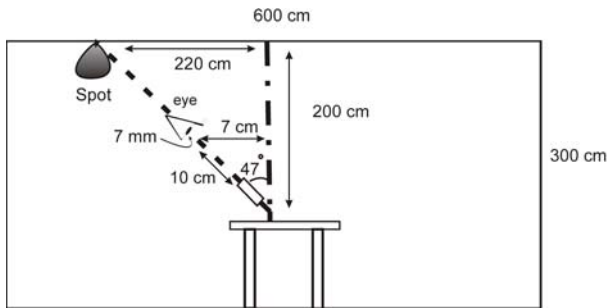
Fig. 3. Geometry of room and eye for the proposed room for the calculation of power gain due to scanning nature DSD emissions.

Fig. 4. Top down view of single spot path and four locations in the room: A (230 cm , 230 cm, 100 cm), B (180 cm, 180 cm, 100 cm), C (90 cm, 90 cm, 100 cm) and D (5 cm, 5 cm, 100 cm). The origin is assumed to be at the bottom left corner of the room.

Fig. 5. Spot configuration for circular paths with 6 spots used in simulations.

placed on a table with 1 m height and the spot moves on a circular path with radius of 220 cm. From the figure, for the worst case when eye distance from transmitter is 10 cm we have: $C_T^{\text{eye}} \approx 0.7/(2\pi \times 7) = 0.015$. In this example, due to the spot motion the transmitter can increase its amplitude 66 times for the same average optical power which is equivalent to an 18 dBo gain in optical power when the spot is in the receiver FOV. This significant power gain mitigates some of the power loss inherent in optical wireless systems and allows DSD systems to work over larger ranges and at higher rates than fixed beam systems.

Note that the above improvement in the transmitted amplitude for a given P may be optimistic since it is necessary ensure that the peak optical power is still at a safe level. For high-speed laser systems, the average power limit is by far the most restrictive one. For example, in [29], it is shown that the peak optical power level is 12 dB higher than average optical power for a commercial IrDA transceiver. Thus, significant gains in average optical power can be realized by such a system while ensuring that the peak constraint is also satisfied. The final class of device and available gains must be verified by measurement. Additionally, scanning laser systems must have a safeguard designed to stop emissions in the event of a failure causing beam motion to cease.

D. Improving C_T

As shown in (5), the capacity of a DSD link at each point in the room also depends on the proportion of time the spot is in the receiver FOV, i.e., C_T. The value of C_T depends both on the receiver FOV and spot path. As discussed in Sec. II-C, a multi-element imaging receiver can be employed to simultaneously have a large FOV while maintaining a high sensitivity. The goal of system design is to select a spot path that ensures a near uniform and high capacity over all points in the room. In [30], four different spot paths (linear, circular and two Lissajous paths) are considered for a square room. The circular path is demonstrated as having a high mean and low variance C_T for this application. Additionally, the implementation of a circular path is simple and hence, in this work a circular path is employed in simulations. Fig. 4 shows a single spot path.

Another technique to improve C_T is to use transmitters with multiple spots. Additional spots should be added to improve the C_T distribution over the room. Multi-spot configurations with 2, 4, and 6 spots are considered in this paper where
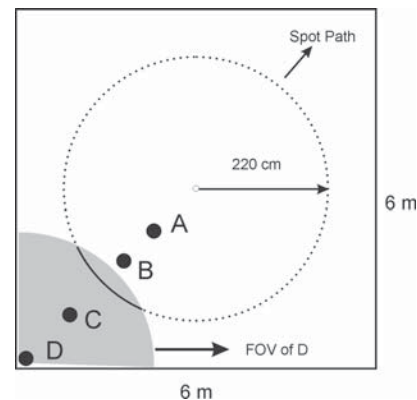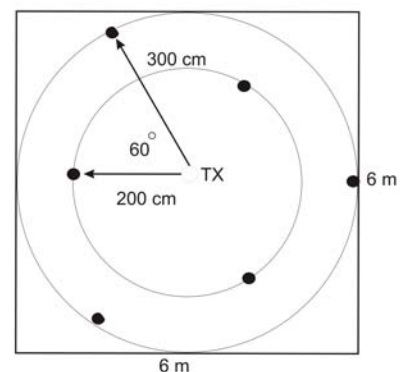
half of the spots have radius of 200 cm and the other half have radius of 300 cm. The n spots have equal phase shifts of $2\pi/n$ and the spots are distributed on different radiuses to avoid multiple spots in one receiver FOV. Figure 5 shows a six spot arrangement considered in this work. The addition of multiple spots increases the mean and decreases the variance of C_T over the room for a moderate increase in complexity.

Note that although additional spots are present, the DSD channel with multi-element receivers and SBC still has a wide bandwidth since the few added spots do not increase the multipath signal significantly. For example, with 6 spots, the simulated DSD system in Sec. II-A maintains a bandwidth higher than 10 GHz. However, as shown in [10], [15], using multiple spots and single-element receiver, the channel bandwidth can be severely limited due to multipath signals received from different spots. However, using SBC with multi-element imaging receivers the receiver only selects at most one spot and the signals received from the others are ignored. Therefore, for multi-element imaging receivers using SBC, having more than one spot in the FOV does not incur additional multipath distortion. However, it must be noted that SBC does have a small SNR penalty over MRC which reduces as the number of imager elements increases [26]. In this work, we assume a multi-element imaging receiver using SBC is employed which mitigates the multipath problem at a small cost of SNR.

III. CHANNEL CODING

As shown in Sec. II, the DSD channel is well approximated as an erasure channel with erasure probability $1 - C_T$ when the received SNR is high. In previously reported systems, the SNR in imaging spot diffusing systems can be made significant, in excess of 15.5 dB, through proper design [12], [13], [17], [18]. For example, in a DSD system with circular spot path and FOV=11.2° similar to the work of Kavehrad [15], an SNR= 10.5 dB results in $C_{\text{in}}^{\text{avg}} = 0.9977$. Considering the MSD system proposed in [12], an SNR= 15.5 dB is available at the receiver resulting in $C_{\text{in}}^{\text{avg}} = 1 - 1.2238 \times 10^{-10}$. Therefore, for the range of SNRs apparent in previous spot diffusing channels, we can consider $C_{\text{in}}^{\text{avg}} \approx 1$ and the DSD channel capacity is approximately C_T. In order to approach this channel capacity, erasure correcting codes must be developed.

Fixed-rate erasure correcting codes, such as Reed-Solomon (RS) codes, are popular in a host of communication and storage applications. However, since the DSD channel capacity is a strong function of position, the application of fixed rate codes, such as RS codes, is not practical. Firstly, in order to design fixed-rate codes, the capacity of the each position in the room must be known *a priori* to the transmitter, which is an impractical situation. Therefore, a different rate code must be designed for each position. Further the number of operations to encode and decode RS codes is proportional to the data block size. This makes such codes practical for relatively small block sizes such as byte error correcting codes of length 256. Thus, fixed-rate codes are completely inappropriate for DSD channels due to the varying channel capacity.

A. Rateless Codes

Rateless codes are a relatively new class of erasure correcting codes. The transmitter in this code is often termed a *digital fountain* since it emits "droplets" of data packets continuously from a given message source [31]. The receivers act as droplet collectors. The entire k packet message can be decoded once a given receiver has collected slightly more than k packets. It is not important which of the emitted packets are received, rather their number is important. As a result, these codes are termed *rateless* since an infinite number of coded packets can be generated from a given data block. Digital Fountain Inc. [32] has proposed commercial rateless codes for many erasure channels, such as packet networks, digital video distribution, software update protocols and also for file storage.

In this work, we apply a rateless code, called an *LT code* [33], to the DSD channel to approach the capacity of the channel. Originally invented by Luby, LT codes generate an infinite stream of data packets from a given data block of k packets. These packets are emitted from the moving spot of the DSD emitter and collected by receivers in the room. At each receiver, the entire message can be decoded, with high probability, when slightly more that k packets are collected [33]. The transmitter does not require any channel information in order to construct the packets. The code rate is adapted automatically depending on the position of receivers in the
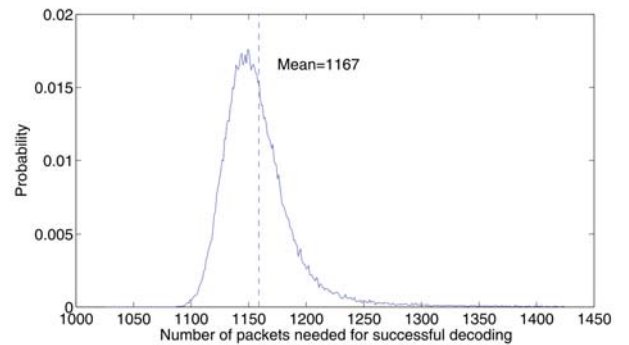
Fig. 6. Probability distribution of packets required for successful decoding, $\rho_p(k')$, for $k = 1024$, $c = 0.05$, $\delta = 0.2$ over 10000 blocks.

room. Additionally, a single transmitter code can be used to simultaneously communicate to all points in the room.

The transmitted packets are generated by taking the exclusive-OR of a random number of message packets selected uniformly with degree selected by a robust soliton distribution [33], [34]. At the receiver, it is assumed that the degree of each packet and its interconnection information are known *a priori* or is encoded in the header of the packet. In this work, instead of sending the entire interconnection information, we assume that identical pseudo-random number generators are available in the transmitter and the receiver. Thus, only the *seed* and the packet degree is required by the decoder to reproduce the same random sequence of selected message packets. In Sec. III-B the format of the transmitted packets is presented. Simplified belief propagation is applied at the receiver to decode the information.

The performance of the LT code depends on the degree distribution, parameterized by c and δ, as well as on the packet size k [33], [35]. The number of the packets required to decode the k input packets, k', is random with probability distribution denoted $\rho_p(k')$ which depends on the code parameters k, c and δ. For example, Fig. 6 shows the probability distribution of $\rho_p(k')$ for $k = 1024$, $c = 0.05$ and $\delta = 0.2$. Since k' is random, so too is the code rate for LT codes. The expected code overhead, denoted α, is defined as $E\{k'\}/k$, i.e., the ratio of the mean number of received packets required to decode the message and the message length. For instance, the mean of k' shown in Fig. 6 is 1167, hence, $\alpha = 1167/1024 = 1.14$. Note that in the figure, to speed simulation the robust soliton distribution was discretized. The value of α quantifies the amount of overhead incurred by the LT code and depends on the code parameters k, c and δ. The overhead can be decreased to achieve a higher data rate by tuning these parameters, however, as α approaches 1 the complexity of the code increases [33], [34]. Therefore, there is a trade-off between complexity and rate.

Rateless codes are based on the assumption of an erasure channel, i.e., packets are received completely and without any error or are totally lost [33], [35]. An effective way to detect packet errors is to employ cyclic redundancy check (CRC) codes. These codes are shortened Hamming cyclic codes [36] and are widely used in Internet and data storage purposes as error detectors. For example, they are used in IEEE 802.3

gigabit Ethernet standard [37]. In the CRC encoder, a *frame check sequence* (FCS) of the input data is computed and is attached to the data packet and used at the receiver for error detection. CRC codes provide strong error detection capability and can be implemented using simple and fast shift register circuits. For example, a 10 Gbps CRC design has been demonstrated [38]. The probability of undetectable error using CRC-32 is shown to be less than 10^{-15} for channel bit error probability $< 10^{-6}$ with packet lengths as long as 12144 bits [39]. The CRC can also be used to detect when the spot is in the FOV of the DSD receiver since the probability that a random sequence satisfies the CRC-32 checksum is negligibly small.

B. Packet Format

The packet format of the DSD system, shown in Fig. 7, is determined both by the data to be transmitted as well as the requirements of the CRC-32 and LT codes. Every packet of length N is composed of a header portion of length m bits and a data portion of length $l = N - m$ bits. The header consists of three parts: the CRC FCS, a seed value and the packet degree. The size of the FCS is fixed at 4 bytes. Together the seed and packet degree contain the interconnection information for the packet. As mentioned earlier, a 4-byte seed value is used to initialize a pseudo-random generator at the receiver with the correct state. Once initialized, the generator produces the sequence of interconnected packets by clocking it according to the degree of the packet. Thus, $m = \log_2 k + 32 + 32$ bits.

The size of the data portion of the packet, l, must be carefully selected to maximize the rates of the DSD channel. In order to increase the data bit rate, the ratio $l/(l + m)$ must be increased, i.e., the overhead of the codes should be small. Since the header is of fixed size, the impact of the overhead of the codes can be made small by increasing l. However, as l increases the probability that a packet is corrupted by the channel noise increases. Let P_{packet} denote the probability that a packet is rejected by the CRC when the spot is in the FOV of the receiver, i.e., that the packet is corrupted by the channel noise. It is simple to justify that $P_{\text{packet}} = 1 - (1 - p)^{l+m}$ where p is the channel bit error rate (BER) $p = Q(\sqrt{\text{SNR}})$ where $Q(x) = \int_x^\infty \exp(-u^2/2)/\sqrt{2\pi}\, du$. When the spot is in the receiver FOV on average $1 - P_{\text{packet}}$ proportion of received packets are not dropped by CRC-32 and can enter the LT decoder. Therefore, increasing l results in increasing P_{packet} and causes the drop out of a greater fraction of received packets, decreasing the data rate.

The trade-off in the packet size l, can be quantified through the average data rate of the DSD link, R_{DSD}. The transmitter emits data at a rate of R_b bits/second by modulating the moving spot and the spot is in the FOV of the receiver C_T fraction of the time. Once the spot is in the receiver FOV, the LT decoder requires on average αk packets to decode the k data packets which form the message. In addition, in every encoded packet $l/(m+l)$ proportion is data. Also, $1 - P_{\text{packet}}$ fraction of packets are not corrupted by noise and are allowed by the CRC-32 to enter the LT decoder. Collecting these factors yields the average data rate of the DSD channel using both CRC-32 and LT codes as

$$R_{\text{DSD}} = (1 - P_{\text{packet}}) \cdot \frac{l}{m + l} \cdot \frac{1}{\alpha} \cdot C_T \cdot R_b. \qquad (7)$$

Considering the extreme limits for l, it is clear that $R_{\text{DSD}} \to 0$ as $l \to 0$ and $l \to \infty$. When $l \to 0$, no data is sent over the channel and when l gets very large, all the packets are corrupted and dropped by the CRC-32. Therefore, there is a optimum value of data portion l which maximizes the data rate. This optimum value depends on the SNR available when the spot is in the receiver FOV. In Sec. IV, the selection of packet size is performed for a given room and channel SNR.

Another potential packet loss occurs when the spot crosses the FOV borders, and a packet may be truncated and so dropped by the CRC check. With the small packet sizes considered in this work due to complexity constraints, the number of received packets in each period is far greater than those truncated when the spot enters and exits the receiver FOV. As a result, the fraction of packets dropped due to this effect is negligible as confirmed in simulation and hence is not explicitly addressed in design.

IV. SIMULATION RESULTS

In this section, simulation results are presented for a DSD system in a typical room. The design of the packet length and the resulting data rates for a variety of locations and transmitter bit rates are estimated by way of simulation and DSD is shown to be a good topology for high-speed indoor wireless optical links.

A. Assumptions and Definitions

In these simulations, we consider a $6 \times 6 \times 3$ m room used in the works of Kavehrad *et al.* [14], [15], [40]. The room reflectivities are assumed to be 0.7, 0.6 and 0.2 for ceiling, walls and floor respectively as in [13]. The spot path is chosen to be a circular path with radius 2.2 m for single spot case which minimizes the blind points in the room, as shown in Fig. 4. In order to quantify the impact of number of spots on rates, as in Sec. II-D, spot paths with 2, 4 and 6 spots are also considered, as shown in Fig. 5. A spot angular speed of 10 Hz is taken as a practical choice and results in a spot motion period $T_s = 0.1$ s.

The receiver FOV is assumed to be $45°$, as the receiver in [12]. The receiver detector diameter is 22 mm. It is a multi-element imaging receiver with 37 pixels and employs SBC technique for combining the outputs. This receiver is employed in the DSD system because it has the largest reported FOV for spot diffusing links and a large FOV multi-element imaging receiver is critical for the DSD system as discussed in Sec. II-D. A previously reported LT code with $k = 1024$, $c = 0.05$ and $\delta = 0.2$ was applied to the DSD channel [34]. A high-speed IEEE 802.3 CRC-32 code from the Ethernet standard is employed to detect and drop corrupted packets [37].

The transmitter sends OOK modulated data at 100 Mbps through a low divergence eye safe beam to a spot on the ceiling. Each beam has an average optical power of 75 mW and employs infrared signals in the 806 nm wavelength region.
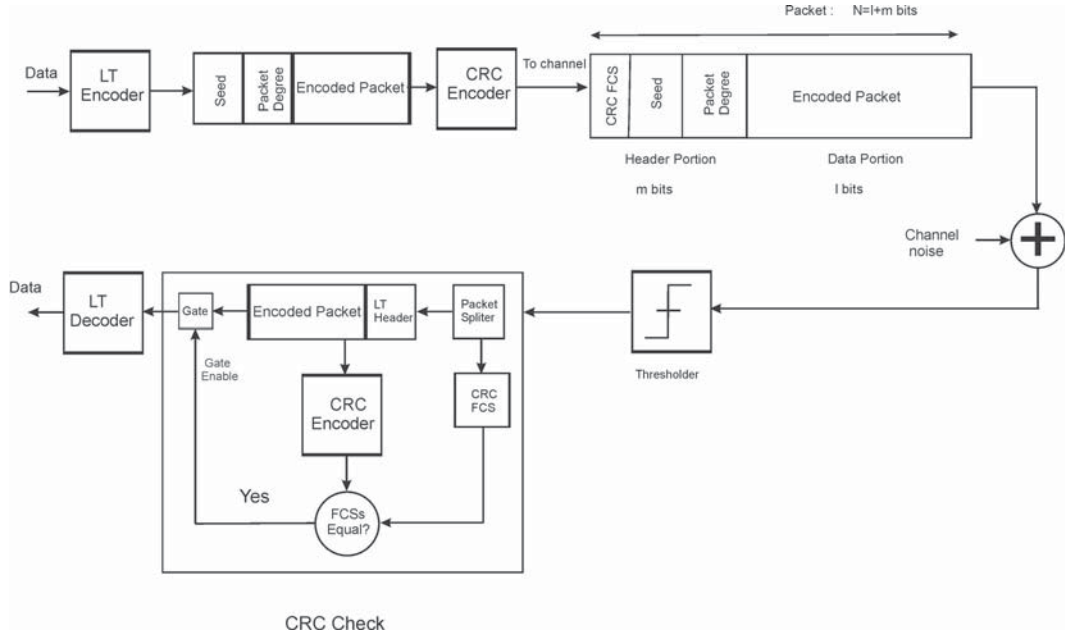
Fig. 7.   The DSD coding system.

TABLE I
ESTIMATED RATES, R_{DSD}/R_b, AND C_T FOR SIMULATED POSITIONS IN
FIG. 4 WITH 1, 2, 4 AND 6 SPOTS AND SNR= 15.5 DB.

Number of Spots	1	2	4	6
C_T for A	0.3	0.56	1	1
C_T for B	0.31	0.6	1	1
C_T for C	0.23	0.46	0.91	1
C_T for D	0.1	0.14	0.28	0.42
R_{DSD}/R_b for A	0.25	0.47	0.84	0.84
R_{DSD}/R_b for B	0.26	0.50	0.84	0.84
R_{DSD}/R_b for C	0.2	0.38	0.76	0.84
R_{DSD}/R_b for D	0.08	0.12	0.23	0.35

Fig. 8.   Normalized rates, $R_{\mathrm{DSD}}/(C_T \cdot R_b)$, for three channel SNRs versus packet size, N. Simulated points are shown by '$*$' while the solid lines are the rates predicted by (7).

The spot diameter on the ceiling is 5 cm. The uncoded probability of error in this configuration, p, is reported to be 10^{-9} [12] in the presence of bright sunlight and thus, the SNR at the receiver is at least 15.5 dB.

As shown in Fig. 4, four positions with high, moderate and low C_T in this room are chosen and the achieved rates are computed for different transmitter bit rates. Table I shows the C_T for these positions using 1, 2, 4 and 6 spots arranged as in Figs. 4 and 5. It is assumed that receivers are able to send a single bit of feedback to the transmitter when the current message has been correctly decoded. The feedback can occur via a diffuse optical channel, as in [6], or using a low data rate radio channel. The transmitter will continue sending encoded packets generated from a given data block until told to stop from the receiver.

B. Numerical Results

1) Packet Size Selection: In order to design the packet length, l, the DSD coding system in Fig. 7 was simulated for various packet sizes and SNRs in order to validated the predicated rates in (7). Packets sizes of $N > 1000$ bytes are not considered in this work because the complexity of the LT encoder and decoder depends linearly on packet size.

Figure 8 presents the simulated and predicted normalized rate $R_{\mathrm{DSD}}/R_b C_T$ versus packet size, N. The simulation results are shown by '$*$' while the expected rates obtained by (7) are plotted within a solid line. As it can be seen from the figure, the simulation results are consistent with the rates predicted by (7). Notice that for each SNR there is an optimum packet size which balances the rate loss due to overhead with the probability of error. As the SNR at the receiver when the spot is in the FOV increases the optimum packet size also increases. Notice that the difference between the performance when SNR= 15.5 dB and 13.5 dB is not significant since P_{packet} is small in both cases and few packets are dropped out by CRC due to the channel noise. In further simulations the packet size is set to $N = 200$ bytes. The goal is to select a packet size which is small, to minimize receiver complexity, while operating near the optimum rate point. As shown in Fig. 8, this packet size achieves high rates for a wide range of SNRs and the complexity of implementation is held to a moderate level.

2) Rate Estimates: The data rate for each position in Fig. 4 can be computed from (7) for the case of SNR=15.5 dB. Table I presents the computed normalized rates, R_{DSD}/R_b, at the proposed positions for these links as well as the C_T for each location. As discussed in Sec. II-B, in the high SNR regime, the DSD channel capacity is approximately equal to C_T. Notice that for the four locations studied, the DSD coding system was able to achieve a significant fraction of the underlying channel capacity. A gap between C_T and the achieved normalized rates in Table I exists due to the overhead inherent in the coding and decoding process. A small additional rate loss also occurs due to the packets corrupted by the channel noise and subsequently dropped by CRC-32 code, as discussed in Sec. III-B.

Notice the dramatic increase in rate when the number of spots increases from 1 to 6 in Table I. This increase in rate mirrors a complementary increase in C_T for each position in the room. The selection of spot path and the number of spots are critical parameters which must be adapted for each room setting in order to maximize rates. Unlike MSD links, however, the DSD architecture is able to provide high data rates throughout the room with a small number of transmitter elements. For a given location, in order to increase rates (7) suggests that the LT code overhead α must decrease and l should be increased. As discussed in Sec. III-A, it is possible to decrease α at the expense of additional complexity.

Another technique to increase data rates is to increase the rate of the transmitter. Consider a DSD link with a transmitter which is able to modulate data onto the spot at a rate of $R_b = 1$ Gbps. Although an experimental spot diffusing channel working at this rate has not yet been reported, optical devices working in this rate are available and an experimental LOS link working at 1 Gbps has been reported [41]. In addition, ongoing experimental work into the development of gigabit-per-second multi-element imaging receivers for optical wireless is taking place [27]. Consider such a link in which the transmitter power level is assumed to be equal to the eye safe 100 Mbps link. Assume that a multi-element imaging receiver is available at 1 Gbps with noise power spectral density the same as in the 100 Mbps link. Therefore, the SNR changes due to the increased bit rate, as in (2) and changing the rate from 100 Mbps to 1 Gbps results in a 10 dB decrease in received SNR. In order to compensate for a portion of this SNR loss, power efficient modulation such as L-PPM can be employed. As discussed in Sec. II-C, L-PPM modulation uses the wide bandwidth available in DSD links to increase power efficiency. Since the bandwidth of the DSD channel is in excess of 10 GHz as presented in Sec.II-A, the channel can still be considered flat in the band of interest. For example, employing 8-PPM which requires 2.6 times the bandwidth of OOK and allows transmitting 5.4 dBo more optical power. From (2), this corresponds to and SNR increase of 10.8 dB and the received SNR would be $15.5 - 10 + 10.8 = 16.3$ dB. Thus, the use of power efficient modulation in this example can compensate the SNR loss due to the increase in R_b and the normalized rates will be approximately as the previous link, shown in Table I. Theoretically, with the 1 Gbps transmitter rates in the range of 350-840 Mbps would be available at the various points in the room. Of course, this analysis assumes sufficient processing resources to accommodate the higher bit rate.

As a limiting case, consider that the data rate of the transmitter is further increased to $R_b = 10$ Gbps. As discussed in Sec. II, the DSD channel bandwidth extends beyond 10 GHz and thus it may be possible to a employ multi-GHz transmitters in the DSD channels. As was done previously, assume than a multi-element imaging receiver working at this rate is available where noise spectral density is not changed by operating at 10 Gbps. Although such a receiver working at 10 Gbps has not been reported yet, the essential components for such a link are available, such as 10 Gbps commercial VCSEL and APDs. In this case, (2) shows that the SNR would decrease 20 dB compared to the 100 Mbps link. Employing power efficient L-PPM modulation to compensate this loss is not practical due to this extremely high order required.

However, as shown in Sec. II-C, the spot motion in the DSD system creates a scanning laser system which permits an increase in the transmitted average optical power while remaining eye safe. For example, it is shown in Sec. II-C that for the room considered and a circular path, using (6), it is estimated that it is possible to send 18 dBo more average optical power in the transmitter. In order to achieve the same 15.5 dB SNR as in the 100 Mbps link, the average optical power needs to be increased by 10 dBo to overcome the SNR loss due to increase in rate. Notice that each dBo increase in optical power corresponds to 2 dB increase in the SNR (2). Hence, using this configuration, the achieved normalized rates are the same as those in Table I and the achieved rates using 6 spots varies between 3.5-8 Gbps.

V. CONCLUSIONS

In this paper, the DSD configuration for wireless optical networks is proposed which combines mobility and high bit rate. Unlike diffuse links where bit rate is limited by multipath dispersion, DSD channels have a multi-GHz bandwidth. These DSD links share many of the benefits of previously proposed MSD links and have the benefit of having a flexible and simple transmitter which can be easily adapted to various room configurations. The SNR loss inherent in high-speed optical wireless systems can be largely compensated for in DSD systems due to their scanning nature and wide bandwidth which permits the use of power efficient modulation.

A DSD link can be built with inexpensive translating mirrors or a rotating motor. By controlling the motor or mirror orientation and speed the DSD spot path can be adapted for individual rooms. This is unlike MSD links which require computer generated holograms [14] which must be designed for a specific location and room size. Although the transmitter design in DSD links is simpler and more flexible than MSD, DSD links have greater complexity in receiver design due to the necessity of using erasure correcting codes. We have shown in this paper through simulation that rates in the range of 8-25 Mbps are possible using DSD links using only a single spot modulated at 100 Mbps and rates of 230-840 Mbps are possible using four spots and a 1 Gbps modulator.

The DSD channel is an attractive configuration for multi-cast indoor optical wireless networks since it is inexpensive,

flexible and has a high data rate. Particularly, it can be used for indoor multimedia broadcasting and down-link internet channel. Current work centers on the development of low complexity codes to jointly combat noise and erasure, the use of higher rate Raptor codes and on the implementation of an experimental DSD link.

ACKNOWLEDGMENT

REFERENCES

[1] F. R. Gfeller and U. Bapst, "Wireless in-house communication via diffuse infrared radiation," *Proc. IEEE*, vol. 67, no. 11, pp. 1474–1486, Nov. 1979.

[2] R. R. Valadas, A. R. Tavares, A. M. de Oliveira Duarte, A. C. Moreira, and C. T. Lomba, "The infrared physical layer of the IEEE 802.11 standard for wireless local area networks," *IEEE Commun. Mag.*, vol. 36, no. 12, pp. 107–112, Dec. 1998.

[3] F. Gfeller and W. Hirt, "Advanced infrared (AIr): physical layer for reliable transmission and medium access," in *Proc. IEEE Int. Seminar Broadband Commun. Zurich*, 2000, pp. 77–84.

[4] T. S. Chu and M. J. Gans, "High speed infrared local wireless communications," *IEEE Commun. Mag.*, vol. 25, no. 8, pp. 4–10, Aug. 1987.

[5] F. Parand, G. E. Faulkner, and D. C. O'Brien, "Cellular tracked optical wireless demonstration link," *IEE Proc. Optoelectron.*, vol. 150, no. 5, pp. 490–496, Oct. 2003.

[6] V. Jungnickel, A. Forck, T. Haustein, U. Kruger, V. Pohl, and C. von Helmolt, "Electronic tracking for wireless infrared communications," *IEEE Trans. Wireless Commun.*, vol. 2, no. 5, pp. 989–999, Sept. 2003.

[7] D. C. O'Brien, G. E. Faulkner, K. Jim, E. B. Zyambo, D. J. Edwards, M. Whitehead, P. Stavrinou, G. Parry, J. Bellon, M. J. Sibley, V. A. Lalithambika, V. M. Joyer, R. J. Samsudin, D. M. Holburn, and R. J. Mears, "High-speed intergrated transceivers for optical wireless," *IEEE Commun. Mag.*, Mar. 2003.

[8] G. Yun and M. Kavehrad, "Spot-diffusing and fly-eye receivers for indoor infrared wireless communications," in *Proc. IEEE Int. Conf. Sel. Top. in Wireless Commun.*, pp. 262–265, 1992.

[9] Y. A. Alqudah and M. Kavehrad, "MIMO characterization of indoor wireless optical link using a diffuse-transmission configuration," *IEEE Trans. Commun.*, vol. 51, no. 9, pp. 1554–1560, Sept. 2003.

[10] S. T. Jivkova, B. A. Hristov, and M. Kavehrad, "Power-efficient multispot-diffuse multiple-input-multiple-output approach to broad-band optical wireless communications," *IEEE Trans. Veh. Technol.*, vol. 53, no. 3, pp. 882–889, May 2004.

[11] S. T. Jivkova and M. Kavehrad, "Multispot diffusing configuration for wireless infrared access," *IEEE Trans. Commun.*, vol. 48, no. 6, pp. 970–978, June 2000.

[12] J. M. Kahn, R. You, P. Djahani, A. G. Weisbin, B. K. Teik, and A. Tang, "Imaging diversity receivers for high-speed infrared wireless communcation," *IEEE Commun. Mag.*, pp. 88–94, Dec. 1998.

[13] J. Carruthers and J. M. Kahn, "Angle diversity for nondirected wireless infrared communications," in *Proc. IEEE Intl. Conf. Commun. ICC*, vol. 3, pp. 1665–1670, June 1998.

[14] M. Kavehrad and S. Jivkova, "Indoor broadband optical wireless communications:optical subsystems design and their impact on channel characteristics," *IEEE Wireless Commun. Mag.*, pp. 30–35, Apr. 2003.

[15] S. Jivkova and M. Kavehrad, "Receiver designs and channel characterization for multi-spot high-bit-rate wireless infrared communications," *IEEE Trans. Commun.*, vol. 49, no. 12, pp. 2145–2153, Dec. 2001.

[16] V. Jungnickel, C. von Helmolt, and U. Kruger, "Broadband wireless infrared LAN architecture compatible with ethernet protocol," *Electron. Lett.*, vol. 34, no. 25, pp. 2371–2372, Dec. 1998.

[17] A. G. Al-Ghamdi and J. M. H. Elmirghani, "Line strip spot-diffusing transmitter configuration for optical wireless systems influenced by background noise and multipath dispersion," *IEEE Trans. Commun.*, vol. 52, no. 1, pp. 37–45, Jan. 2004.

[18] ——, "Multiple spot diffusing geometries for indoor optical wireless communication systems," *Int. J. Commun. Syst.*, vol. 16, pp. 909–922, 2003.

[19] S. Jivkova and M. Kavehrad, "Transceiver design concept for cellular and multispot diffusing regimes of transmission," *EURASIP J. Appl. Signal Processing*, no. 1, pp. 30–38, 2005.

[20] S. Hranilovic, *Wireless Optical Communication Systems*. New York, NY: Springer, 2004.

[21] J. M. Kahn and J. R. Barry, "Wireless infrared communications," *Proc. IEEE*, vol. 85, pp. 265–298, Feb. 1997.

[22] J. R. Barry, J. M. Kahn, W. J. Krause, E. A. Lee, and D. G. Messerschmitt, "Simulation of multipath impulse response for indoor wireless optical channels," *IEEE J. Select. Areas Commun.*, vol. 11, no. 3, pp. 376–379, Apr. 1993.

[23] A. J. Goldsmith and P. P. Varaiya, "Fading channels: information-thoretic and communications aspects," *IEEE Trans. Inform. Theory*, vol. 43, no. 6, pp. 2619–2692, Oct. 1997.

[24] I. E. Telatar, "Capacity of multi-antenna Gaussian channels," *European Trans. Telecommun.*, pp. 585–595, Nov. 1999.

[25] D. J. C. MacKay, *Information Theory, Inference and Learning Algorithms*. Cambridge University Press, 2004.

[26] P. Djahani and J. M. Kahn, "Analysis of infrared wireless links employing multibeam transmitters and imaging diversity receivers," *IEEE Trans. Commun.*, vol. 48, no. 12, pp. 2077–2088, Dec. 2000.

[27] D. C. O'Brien, G. E. Faulkner, E. B. Zyambo, K. Jim, D. J. Edwards, P. Stavrinou, G. Parry, J. Bellon, M. J. Sibley, V. A. Lalithambika, V. M. Joyner, R. J. Samsudin, D. M. Holburn, and R. J. Mears, "Integrated transceivers for optical wireless communications," *IEEE J. Select. Topics Quantum Electron.*, vol. 11, no. 1, pp. 173–183, 2005.

[28] International Electrotechnical Comission, "Safety of laser products—part 1: equipment classification, requirements and user's guide," group safety publication, reference number 825-1, 1993.

[29] A. C. Boucouvalas, "IEC 825-1 eye safety classification of some consumer electronic products," in *Proc. IEE Colloquium on Optical Free Space Communication Links,*, pp. 13/1–13/6, Feb 1996.

[30] F. Khozeimeh and S. Hranilovic, "A dynamic spot diffusing architecture for indoor wireless optical communications," in *Proc. IEEE Int. Conf. on Commun.*, vol. 6, 2006, pp. 2829–2834.

[31] J. Byers, M. Luby, and M. Mitzenmacher, "A digital fountain approach to asynchronous reliable multicast," *IEEE J. Select. Areas Commun.*, vol. 20, no. 8, pp. 1528–1540, Oct. 2005.

[32] Digital Fountain Inc, "http://www.digitalfountain.com."

[33] M. Luby, "LT codes," in *Proc. Symposium Foundations of Computer Science*, pp. 271–280, 2002.

[34] F. Uyeda, H. Xia, and A. A. Chien, "Evaluation of a high performance erasure code implementation," report prepared for Computer Science and Engineering Department, University of California, San Diego, Sept. 2004.

[35] D. J. C. Mackay, "Fountain codes," *IEE Proc. Commun.*, vol. 152, no. 6, pp. 1062–1068, Dec. 2005.

[36] S. Lin and D. J. Costello, *Error Control Coding: Fundamentals and applications*. Prentice-Hall, 1983.

[37] "IEEE Standard 802.3, part 3: carrier sense multiple access with collision detect on (CSMA/CD) access method and physical layer specifications, 2002."

[38] J. S. Lin, C. K. Lee, M. D. Shieh, and J. H. Chen, "High-speed CRC design for 10 Gbps applications," in *Proc. IEEE Intl. Symposium Circuits and Systems.*, pp. 3177–3180, May 2006.

[39] T. Fujiwara, T. Kasami, and S. Lin, "Error detecting capabilities of the shortened Hamming codes adopted for error detection in IEEE standard 802.3," *IEEE Trans. Commun.*, vol. 37, no. 9, pp. 986–989, Sept. 1989.

[40] M. K. K. Akhavan and S. T. Jivkova, "Wireless infrared in-house communications: Hhow to achieve very high bit rates," in *Proc. IEEE Wireless Communications and Networking*, vol. 2, pp. 698–703, Sept. 2000.

[41] D. R. Wisely, "A 1 Gbit/s optical wireless tracked architecture for ATM delivery," in *Proc. IEE Coll. Opt. Free Space Commun. Links*, London, U.K, pp. 14/1–14/7, 1996.

Farhad Khozeimeh was born in Tehran, Iran, in 1981. He received his B.S. in electrical engineering from Sharif University of Technology in 2004. He started his M.Sc. studies at McMaster University, Hamilton, Canada, where he joined the Free-Space Optical Communication Algorithms Laboratory (FOCAL). His M.Sc. research was on a novel configuration for indoor optical wireless communications, termed Dynamic Spot Diffusing (DSD). His M.Sc. thesis won the Outstanding Thesis award from the department of Electrical and Computer Engineering of McMaster University. Farhad joined Cognitive Systems Laboratory (CSL) at McMaster University in Sep. 2006 where he is currently working toward his Ph.D. degree. His research interests include cognitive radio, wireless communications and machine learning.

Steve Hranilovic received the B.A.Sc. degree with honours in electrical engineering from the University of Waterloo, Canada in 1997 and M.A.Sc. and Ph.D. degrees in electrical engineering from the University of Toronto, Canada in 1999 and 2003 respectively. He is an Assistant Professor in the Department of Electrical and Computer Engineering, McMaster University, Hamilton, Ontario, Canada. From 1992 to 1997, while studying for the B.A.Sc. degree, he worked in the areas of semiconductor device characterization and microelectronics for Nortel Networks and the VLSI Research Group, University of Waterloo. His research interests are in the areas of free-space and wired optical communications, digital communications algorithms, and electronic and photonic implementation of coding and communication algorithms. He is the author of the book *Wireless Optical Communications Systems* (New York: Springer, 2004). Dr. Hranilovic is a licensed Professional Engineer in the Province of Ontario. In 2006, he was awarded the Government of Ontario Early Researcher Award. He is currently the Chair of the joint IEEE Communications/Signal Processing/Information Theory Societies Chapter in the Hamilton Section.